Formation of quasi-free-standing graphene on SiC(0001) through intercalation of erbium

Cite as: AIP Advances **11**, 025314 (2021); https://doi.org/10.1063/9.0000154
Submitted: 21 October 2020 . Accepted: 05 January 2021 . Published Online: 08 February 2021

P. D. Bentley, T. W. Bird, A. P. J. Graham, O. Fossberg, S. P. Tear, and A. Pratt

Formation of quasi-free-standing graphene on SiC(0001) through intercalation of erbium

Cite as: AIP Advances 11, 025314 (2021); doi: 10.1063/9.0000154
Presented: 4 November 2020 • Submitted: 21 October 2020 •
Accepted: 5 January 2021 • Published Online: 8 February 2021

P. D. Bentley, T. W. Bird, A. P. J. Graham, O. Fossberg, S. P. Tear, and A. Pratt[a)]

AFFILIATIONS

Department of Physics, University of York, Heslington West, York YO10 5DD, United Kingdom

Note: This paper was presented at the 65th Annual Conference on Magnetism and Magnetic Materials.
[a)]**Author to whom correspondence should be addressed:** andrew.pratt@york.ac.uk

ABSTRACT

Activation of the carbon buffer layer on 4H- and 6H-SiC substrates using elements with high magnetic moments may lead to novel graphene/SiC-based spintronic devices. In this work, we use a variety of surface analysis techniques to explore the intercalation of Er underneath the buffer layer showing evidence for the associated formation of quasi-free-standing graphene (QFSG). A combined analysis of low energy electron diffraction (LEED), atomic force microscopy (AFM), X-ray and ultraviolet photoemission spectroscopy (XPS and UPS), and metastable de-excitation spectroscopy (MDS) data reveals that annealing at temperatures up to 1073 K leads to deposited Er clustering at the surface. The data suggest that intercalation of Er occurs at 1273 K leading to the breaking of back-bonds between the carbon buffer layer and the underlying SiC substrate and the formation of QFSG. Further annealing at 1473 K does not lead to the desorption of Er atoms but does result in further graphitization of the surface.

I. INTRODUCTION

Graphene's large spin relaxation length at room temperature continues to attract significant attention in terms of potential applications in spintronics.[1] Thermal decomposition of silicon carbide provides a route towards high-quality epitaxial graphene,[2] however is limited for the 4H and 6H-SiC Si polar faces due to subsurface Si back-bonds. These lead to the first carbon layer that forms having the same structure as graphene but acting as a buffer layer that displays no linear dispersion at the K-point in reciprocal space.[3] Adatoms such as H, Ca, Mn, Li, Au, Fe and Co[4–10] have all been used to break these back-bonds, resulting in the formation of "quasi-free-standing graphene" (QFSG),[4] with the additional benefit of potentially enhancing the magnetic properties of this graphene layer.[10]

Specifically, tailoring graphene for spintronic applications generally involves enhancing its intrinsically weak spin-orbit coupling (SOC),[1] either by adatom decoration[11] or through proximity effects.[12] Since the strength of SOC scales with atomic number (Z), there has been increasing research activity related to intercalation/adatom decoration of heavier elements under/on graphene including Au[8] and the lanthanide series.[13–16] In addition to forming QFSG, it is proposed that the high magnetic moment associated with the rare earth metals will lead to enhanced SOC following intercalation providing a route to magnetic storage and other spintronic devices.[13] For example, one such study has shown Eu to intercalate, form a periodic array of atoms underneath the buffer layer and be protected from oxidation for months after being removed from ultra-high vacuum (UHV).[15] To date, Eu, Dy, Yb, and Gd have all been studied,[14–16] although Er intercalation has not yet been reported, despite it having one of the highest magnetic moments (7 μ_B) of all the lanthanides. Additionally, the mechanism of rare-earth interaction with the buffer layer and how intercalation leads to QFSG is not fully understood.

In this work, we explore the intercalation of Er underneath the carbon buffer layer that forms on 6H-SiC(0001) substrates using a variety of surface analysis techniques. In particular, we make use of the extreme surface sensitivity associated with metastable de-excitation spectroscopy (MDS), which we apply here to the study of rare-earth intercalation for the first time.[17,18] The large de-excitation cross-section of helium atoms in the long-lived metastable 2^3S state (19.82 eV) provides access to the outermost electronic and

magnetic structure of a surface providing complementary information to, for example, ultraviolet photoemission spectroscopy (UPS). Together with low energy electron diffraction (LEED), atomic force microscopy (AFM), and X-ray photoemission spectroscopy (XPS) results, the UPS and MDS data reveal that Er intercalates beneath the buffer layer, likely breaking back-bonds to form QFSG and thereby providing a potential system for future studies of SOC enhancement.

II. EXPERIMENTAL TECHNIQUES

Wafers of *n*-type vanadium- and nitrogen-doped 6H-SiC were purchased from Semiconductor Wafer Inc., samples cut, and mounted onto Scienta Omicron GmbH direct-current heating plates with the (0001) silicon-rich face up. Electron spectroscopy measurements were performed in a UHV system consisting of a preparation chamber and an analysis chamber with base pressures of $< 5 \times 10^{-10}$ mbar and $< 1 \times 10^{-10}$ mbar respectively. All spectra were obtained using a Scienta Omicron GmbH EA 125 hemispherical energy analyzer. A Scienta Omicron GmbH VUV HIS 13 cold cathode discharge source was used to generate He I α UV photons ($h\nu$=21.22 eV). Metastable helium 2^3S atoms for performing MDS were produced using a bespoke liquid-nitrogen-cooled direct-current discharge source.[19] Al $K\alpha_1$ (1486.7 ± 0.1 eV) monochromated X-rays were generated using a Scienta Omicron GmbH XM1000 MKII Mono X-ray source. All LEED and LEED I/V measurements were performed in a separate UHV system with a base pressure of $< 1 \times 10^{-10}$ mbar. LEED images were obtained using a Scienta Omicron GmbH SPECTALEED instrument equipped with a LaB_6 filament. LEED I/V measurements were performed using a combination of Neptune and kSA 400 software, and all images were taken using a kSA K-30FW camera. AFM images were obtained on a Bruker BioScope Resolve instrument operating in tapping mode. A buffer layer of carbon was prepared by annealing each SiC sample at 1473 K for 30 minutes, with temperature measured using a Raytek Corp infrared pyrometer. Erbium was deposited using bespoke evaporation sources consisting of erbium lumps mounted in a tantalum boat with deposition rate calibrated using a quartz crystal microbalance.[20]

III. RESULTS

A. Low energy electron diffraction and LEED I/V

Following preparation of the buffer layer, several SiC substrates were covered with 0.5 monolayer (ML) of erbium with the samples at room temperature during growth (ρ = 8.795 gcm^{-3}, thickness of an Er ML τ = 2.36 Å).[21] Following deposition, the $(6\sqrt{3} \times 6\sqrt{3})$ R30°LEED pattern associated with the buffer layer (Figure 1(a)) disappeared at all energies (Figure 1(b)) implying the formation of a disordered Er layer atop the buffer layer. By annealing for 5 minutes in increasing 100 K steps, the $6\sqrt{3}$ LEED pattern was eventually recovered at 1073 K, with a similar LEED I/V curve to that prior to deposition (Figure 1(e)). Partial restoration of the $6\sqrt{3}$ periodicity is consistent with a proportion of the buffer layer again being exposed suggesting that annealing at 1073 K either results in Er desorbing from the surface, or alternatively, Er clustering at the surface. The latter is supported by Vaknin *et al.* who reported Eu to form clusters on the buffer layer over a similar temperature range.[15] To investigate this further, we performed AFM on buffer layer samples exposed to a coverage of 0.5 ML of Er at room temperature with several resulting images shown in Figure 2. At lower magni-

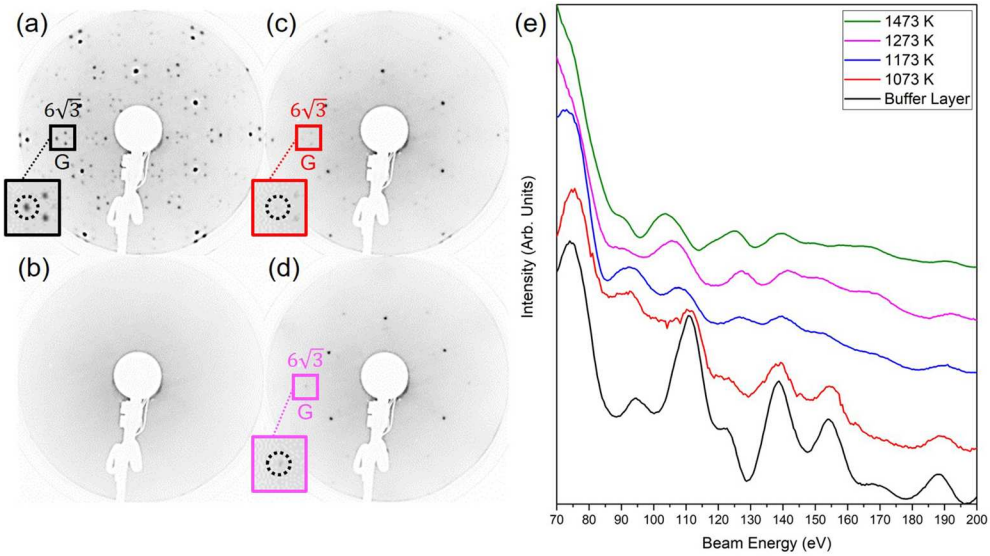

FIG. 1. LEED images taken at 126 eV of (a) the buffer layer and (b) after a 0.5 monolayer deposition of erbium with the 6H-SiC sample at room temperature. Further annealing of the sample was then performed in 100 K steps. After annealing at (c) 1073 K and 1173 K (not shown), the graphene spot (dashed circle) and subsidiary spots of the $6\sqrt{3}$ buffer layer LEED pattern remain but are increasingly diminished. (d) At 1273 K, subsidiary spots associated with the buffer layer have almost disappeared but the graphene spot remains. (e) The evolution of the LEED pattern is reflected in the corresponding LEED I/V spectra of the graphene spot with a pronounced change evident at 1173 K and above.

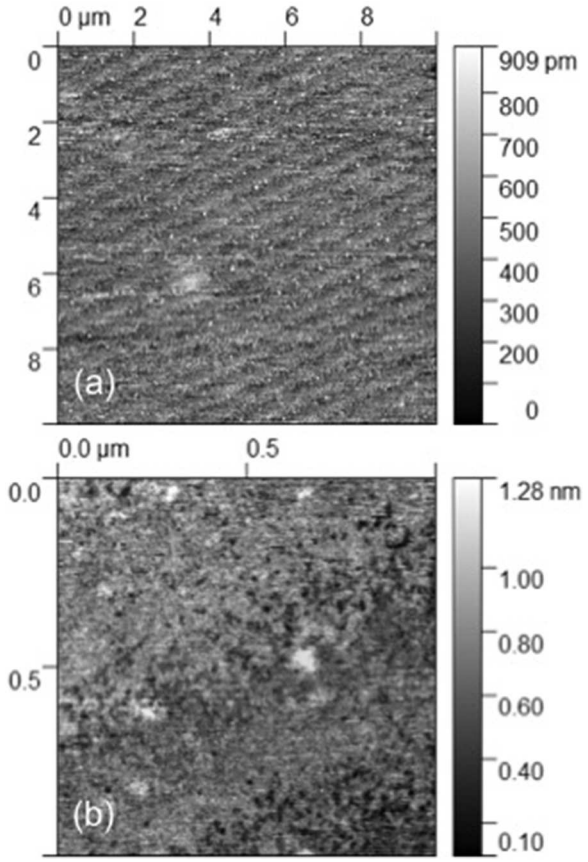

FIG. 2. Atomic force microscopy (AFM) images of a sample of 0.5 ML of Er deposited at room temperature on to a carbon buffer layer prepared on a 6H-SiC(0001) substrate. Clear terraces are observed in the lower magnification image (a) along with bright spots which are shown in greater detail in (b).

fication (Figure 2(a)), clear terraces of the substrate can be seen which have a typical width of ~500 nm and height of ~0.5 nm. Step-edges between terraces appear to be decorated by bright spots which can be seen in more detail in Figure 2(b). Individual atoms are not resolvable in these images but the location and prevalence of these bright spots support Er clustering at disordered step edges of the SiC substrate.

Annealing at 1173 K and above results in further changes to the LEED pattern and associated LEED I/V spectra as seen in Figure 1(d) and (e). The subsidiary $6\sqrt{3}$ spots that surround the graphene spot (dashed circle) are heavily suppressed although the graphene spot itself remains visible. These changes are further reflected in the LEED I/V data where the spectrum after annealing at 1173 K is significantly different from the buffer layer and 1073 K anneal spectra. The most notable changes in the spectra occur in the 70-110 eV energy range where characteristic Bragg peaks indicate the formation of buffer-layer graphene. In particular, the reduction of the peak at ~74 eV for the 1173 K anneal to a shoulder-like feature for higher temperatures indicates the evolution of the buffer layer to monolayer or bilayer graphene.[22] Changes in the LEED I/V spectra at these low energies are indicative of a structural change close to the surface (within the first few atomic sublayers) based on the information depth of electrons within this energy range.

The LEED and LEED I/V data suggest that erbium has either desorbed at 1173 K and above, clustered in a manner so that the buffer layer becomes partially covered, or intercalated underneath the buffer layer. Intercalation of Eu beneath the buffer layer leading to the breaking of Si-C back-bonds following annealing has previously been reported.[15] A similar mechanism of intercalation possibly explains the LEED data for Er presented here. Spots in the LEED pattern associated with the $6\sqrt{3}$ periodicity of the buffer layer mostly disappear after annealing at 1273 K but the graphene spots remain suggesting the formation of QFSG. With a 0.5 ML deposition of Er, it is possible that not all C-Si back-bonds have been replaced by Er-Si bonds so that some regions of buffer-layer graphene remain. Based on this picture, a simplistic schematic of the suggested Er intercalation process is presented in Figure 3.

Annealing at 1473 K does not result in further substantial changes in the LEED I/V spectrum suggesting that Er remains even after heating to such elevated temperatures.[22] In contrast, Vaknin *et al.* observed Eu to "deintercalate" and desorb from the surface at 1473 K although this only followed "prolonged annealing"[16] which results in further graphitization of the sample. As our experiments only involved annealing for 5 minutes at each temperature, it is likely that erbium remained after the 1473 K anneal. It should also be noted that erbium diffusion into the bulk is a possibility, as has been observed for intercalation experiments with other metals.[9]

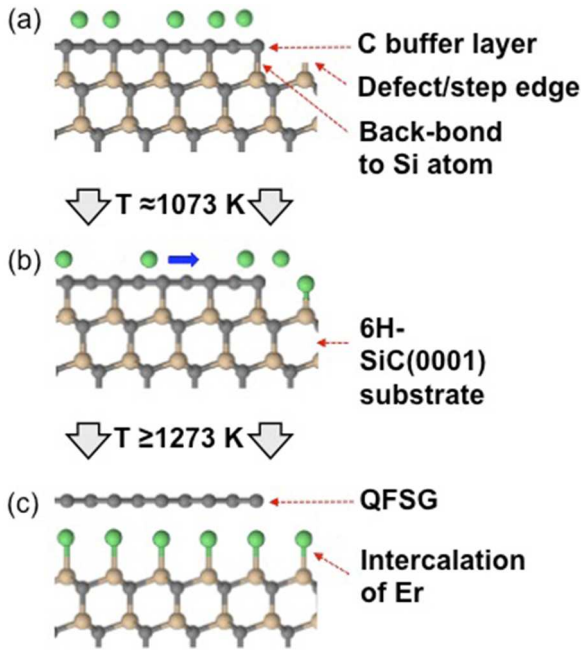

FIG. 3. Schematic representation of the Er intercalation process showing (a) deposition of Er on to a carbon buffer layer formed on a 6H-SiC(0001) substrate, (b) Er migration to defects and step edges after annealing at ~1073 K resulting in cluster formation, and (c) Er intercalation taking place only after annealing above ~1273 K.

B. X-ray photoemission spectroscopy

To help elucidate the behaviour of Er following deposition on the buffer layer, XPS was performed with the results presented in Figures 4 and 5. The peak at ~284.5-285.5 eV in the C 1*s* buffer layer spectrum (Figure 4) arises due to emission from C atoms in this layer, approximately 30% of which are back-bonded to underlying Si atoms at the surface of the substrate.[23] At ~283.3 eV, emission is due to C atoms in the SiC substrate itself. No significant changes to the C 1*s* spectrum are observed following deposition of 0.5 ML of Er with the sample at room temperature or following annealing at 1073 K, consistent with erbium forming clusters at the surface rather than intercalating. Annealing to 1273 K, however, does result in a very different C 1*s* spectrum, with the clear appearance of two peaks in Figure 4 centered at approximately 284.6 eV (i) and 282.6 eV (ii). At an anneal temperature of only 1273 K, such changes cannot be attributed to further graphitization of the surface[3,4] and so are most likely a result of Er strongly interacting with C atoms either in the buffer layer or at the substrate surface. Peak (i) is assigned to C 1*s* emission from the C-C environment present in the QFSG layer in line with previous studies for hydrogen intercalation.[4] The lower energy peak (ii) is at a similar energy to the modified SiC' peak observed for QFSG/bilayer graphene observed by Chung *et al.*[24] Those authors suggested the shift in the peak position occurred as a result of transfer doping from Eu intercalation underneath the buffer layer although other changes in the C environment of the SiC substrate due to intercalation could also contribute to the shift.

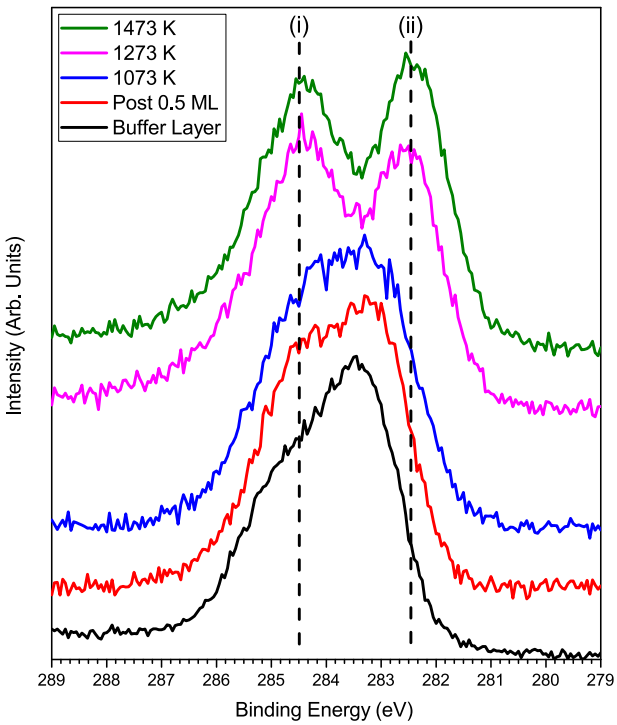

FIG. 4. Normalized XPS spectra of the C 1*s* core state for the buffer layer, following deposition of 0.5 ML of Er with the substrate at room temperature, and following subsequent annealing at 1073, 1273 and 1473 K.

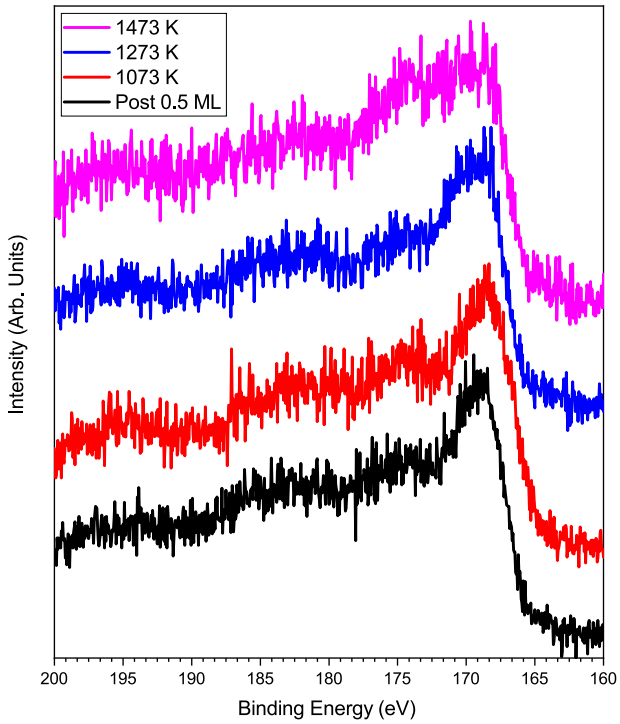

FIG. 5. Normalized XPS spectra of the Er 4*d* core state for the buffer layer, following deposition of 0.5 ML of Er with the substrate at room temperature, and following subsequent annealing at 1073, 1273 and 1473 K.

Figure 5 shows the Er 4*d* core level XPS spectra that correspond to the sample preparation conditions as for the C 1*s* data presented in Figure 4. The complex multiplet structure of the Er 4*d* state makes detailed analysis of the Er bonding environment difficult but the strong peak at a binding energy of ~167-169 eV is characteristic of both metallic Er and Er-Si bonds.[25] The broadening of this peak and subtle shifts in its position as the anneal temperature increases suggest a change in Er bond formation with Er-C bonds typically giving rise to stronger emission at around 170 eV.[26]

Altogether, the XPS results support the occurrence of Er intercalation beneath the buffer layer when annealing at high enough temperatures, likely leading to the breaking of Si-C back-bonds in similarity with Eu intercalation.[15,24] Erbium, as for other intercalated species such as Dy and Au, most likely intercalates through defects in the buffer layer which would lead to the formation of Er-C bonds that may also contribute to the carbide C 1*s* peak.[8,13] Note that the presence of Er even after annealing the sample to 1473 K suggests that Er has not desorbed from the sample to any significant degree.

C. Ultraviolet photoemission spectroscopy and metastable de-excitation spectroscopy

Figures 6 and 7 show respective UPS and MDS spectra corresponding to each step of sample preparation and annealing from the same sample used to obtain the above XPS data. After the Fermi edge at (i) in Figure 6, states (ii) and (iii) at energies of 1.7 and 3 eV

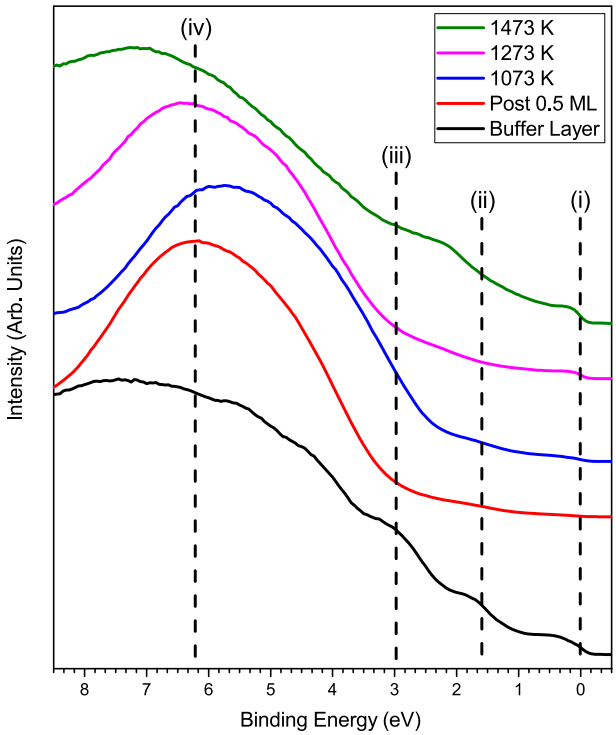

FIG. 6. Normalized UPS spectra of the buffer layer before and after deposition of 0.5 ML of erbium and following subsequent annealing cycles at increasing temperatures.

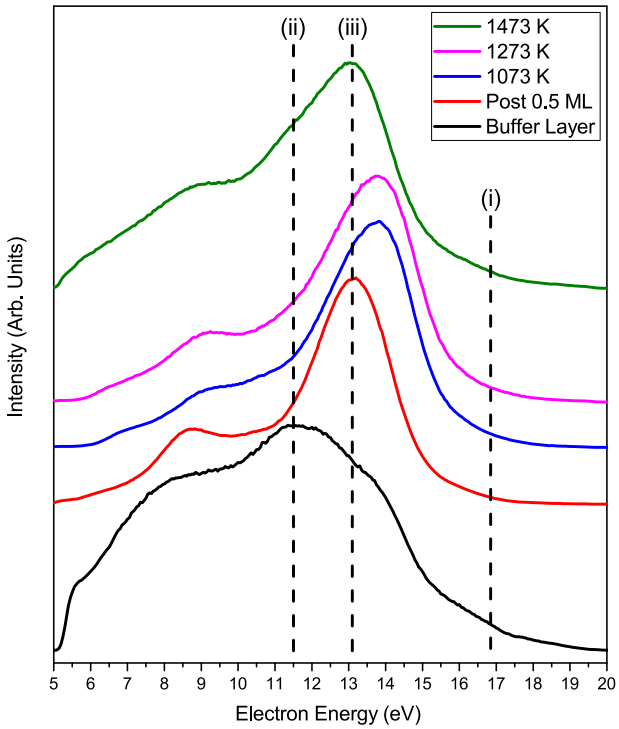

FIG. 7. Normalized MDS spectra of the buffer layer before and after deposition of 0.5 ML of erbium and following subsequent annealing cycles at increasing temperatures.

are features intrinsic to the buffer layer with (ii) arising from the back-bonding state and (iii) due to π-band electrons at the *M* point in reciprocal space.[27] These latter states appear in the MDS spectra of the buffer layer, Figure 7, as a shoulder at approximately 3 eV from the cutoff point, marked (i). Feature (ii) in the buffer layer MDS spectrum at 11.5 eV is associated with π hybridization at the Γ point in reciprocal space.[28] Both of these states are broad as a result of the dominant de-excitation channel for this surface being the two-step process of resonance ionization followed by Auger neutralization.[18]

Deposition of 0.5 ML of erbium leads to significant changes in the UPS and MDS spectra, with features associated with the buffer layer replaced by the formation of a broad peak in both spectra centered around 6.2 - 6.6 eV from the cutoff point. Previous analysis of erbium thin films on homoepitaxial diamond showed that an increase in emission around 5 eV from the Fermi level is a result of Er 4*f* states although it is possible that some emission in this region also occurs due to 2*p* states of oxygen atoms adsorbed on the deposited Er.[29] Annealing the sample at 1073 K results in peak (iv) of the UPS spectrum shifting to a lower binding energy and the partial reappearance of peaks (ii) and (iii), again indicating clustering of Er. Interestingly, these buffer layer features again reduce on annealing to 1273 K which provides further evidence that Er intercalation, and the associated breaking of the C-Si back bonds that give rise to these features, has taken place. Stronger emission at deeper binding energies is possibly a result of the formation of Er-C at defects in the buffer layer, as discussed above. After annealing at 1473 K, the UPS spectrum shows stronger emission at the Fermi level and a new peak at ~2.2 eV indicating graphitization of the sample.[4] The new feature appears at a similar energy to emission observed for $ErSi_2$ arising as a result of the flat part of a band crossing the Γ point in reciprocal space due to an Er atom on a buckled Si top layer site.[30] The formation of Er-Si bonds necessarily means the breaking of back-bonds between C in the buffer layer and Si in the substrate again suggesting the formation of QFSG.

In the MDS spectra, annealing at 1073 K leads to the main peak (iii) moving to a higher kinetic energy suggesting clustering of the deposited erbium atoms. Although both XPS and UPS indicate intercalation of Er atoms occurs after further annealing at 1273 K, the MDS spectrum for this temperature is similar to that at 1073 K. Due to the extreme surface sensitivity of MDS, this indicates that some Er has remained at the surface or is present in relatively large quantities at defected regions of the buffer layer which act as intercalation pathways. Upon annealing to 1473 K, the features in the MDS spectrum evolve to be similar to those for π-band emission from a graphite surface.[18] Together with the UPS data, the MDS results support the picture that Er intercalation occurs following deposition and annealing at sufficient temperatures, in this case 1273 K. Er intercalation leads to bonding with substrate Si atoms and the breaking of C-Si back-bonds leading to the formation of QFSG.

IV. CONCLUSIONS

In this work, we present results from a variety of surface analysis techniques supporting the intercalation of erbium underneath a carbon buffer layer formed on a 6H-SiC(0001) substrate. Upon annealing at temperatures of 1273 K, LEED, XPS, UPS, and MDS all provide evidence that Er intercalation leads to the breaking of subsurface C-Si back-bonds and the formation of quasi-free-standing graphene. Deposition at room temperature initially leads to disordered Er coverage of the buffer layer which then progresses to Er island formation at anneal temperatures below that needed for intercalation. Intercalation likely proceeds through defects in the buffer layer leading to the formation of Er-C bonds. Further investigation, including with complementary techniques such as Raman spectroscopy, will help further elucidate the mechanisms of Er intercalation and the associated changes in the carbon bonding environment. The results presented here suggest an additional way of potentially activating buffer layer graphene using elements with high magnetic moments, possibly providing options for novel graphene/SiC-based spintronic devices.

ACKNOWLEDGMENTS

The authors acknowledge the Engineering and Physical Sciences Research Council (EPSRC) for funding this project (EP/N509802/1). The AFM work was carried out in the York JEOL Nanocentre at the University of York.

DATA AVAILABILITY

The data that support the findings of this study are available from the corresponding author upon reasonable request.

REFERENCES

[1] A. Avsar, H. Ochoa, F. Guinea, B. Özyilmaz, B. J. van Wees, and I. J. Vera-Marun, "Colloquium: Spintronics in graphene and other two-dimensional materials," Rev. Mod. Phys. **92**, 021003 (2020).

[2] D. M. Pakdehi, K. Pierz, S. Wundrack, J. Aprojanz, T. T. N. Nguyen, T. Dziomba, F. Hohls, A. Bakin, R. Stosch, C. Tegenkamp, F. J. Ahlers, and H. W. Schumacher, "Homogeneous large-area quasi-free-standing monolayer and bilayer graphene on SiC," ACS Appl. Nano Mater. **2**, 844–852 (2019).

[3] J. D. Riley, K. V. Emtsev, F. Speck, T. Seyller, and L. Ley, "Interaction, growth, and ordering of epitaxial graphene on SiC{0001} surfaces: A comparative photoelectron spectroscopy study," Phys. Rev. B **77**, 155303 (2008).

[4] C. Riedl, C. Coletti, T. Iwasaki, A. A. Zakharov, and U. Starke, "Quasi-free-standing epitaxial graphene on SiC obtained by hydrogen intercalation," Phys. Rev. Lett. **103**, 246804 (2009).

[5] Y. Zhang, H. Zhang, Y. Cai, J. Song, D. Qiao, Q. Chen, F. Hu, P. Wang, K. Huang, and P. He, "Calcium intercalation underneath N-layer graphene on 6H-SiC(0001)," Chem. Phys. Lett. **703**, 33–38 (2018).

[6] J. Hwang, J.-E. Lee, M. Kang, B.-G. Park, J. Denlinger, S.-K. Mo, and C. Hwang, "Gapped nearly free-standing graphene on an SiC(0001) substrate induced by manganese atoms," Appl. Sci. Converg. Technol. **27**, 90–94 (2018).

[7] M. Omidian, N. Néel, E. Manske, J. Pezoldt, Y. Lei, and J. Kröger, "Structural and local electronic properties of clean and Li-intercalated graphene on SiC(0001)," Surf. Sci. **699**, 121638 (2020).

[8] A. Bayani and K. Larsson, "Intercalation of Au atoms into SiC(0001)/buffer interfaces–A first-principles density functional theory study," ACS Omega **5**, 14842–14846 (2020).

[9] K. Shen, H. Sun, J. Hu, J. Hu, Z. Liang, H. Li, Z. Zhu, Y. Huang, L. Kong, Y. Wang, Z. Jiang, H. Huang, J. W. Wells, and F. Song, "Fabricating quasi-free-standing graphene on a SiC(0001) surface by steerable intercalation of iron," J. Phys. Chem. C **122**, 21484–21492 (2018).

[10] R. Hönig, P. Roese, K. Shamout, T. Ohkochi, U. Berges, and C. Westphal, "Structural, chemical, and magnetic properties of cobalt intercalated graphene on silicon carbide," Nanotechnology **30**, 025702 (2018).

[11] J. Balakrishnan, G. K. W. Koon, M. Jaiswal, A. H. C. Neto, and B. Özyilmaz, "Colossal enhancement of spin–orbit coupling in weakly hydrogenated graphene," Nat. Phys. **9**, 284 (2013).

[12] F. Calleja, H. Ochoa, M. Garnica, S. Barja, J. J. Navarro, A. Black, M. M. Otrokov, E. V. Chulkov, A. Arnau, A. L. V. de Parga, F. Guinea, and R. Miranda, "Spatial variation of a giant spin-orbit effect induces electron confinement in graphene on Pb islands," Nat. Phys. **11**, 43 (2014).

[13] X. Lu, Y. Liu, M. Shao, and X. Liu, "Defect-mediated intercalation of dysprosium on buffer layer graphene supported by SiC(0001) substrate," Chem. Phys. Lett. **742**, 137162 (2020).

[14] M. Kim, M. C. Tringides, M. T. Hershberger, S. Chen, M. Hupalo, P. A. Thiel, C.-Z. Wang, and K.-M. Ho, "Manipulation of Dirac cones in intercalated epitaxial graphene," Carbon **123**, 93–98 (2017).

[15] N. A. Anderson, M. Hupalo, D. Keavney, M. C. Tringides, and D. Vaknin, "Intercalated europium metal in epitaxial graphene on SiC," Phys. Rev. Materials **1**, 054005 (2017).

[16] N. A. Anderson, M. Hupalo, D. Keavney, M. Tringides, and D. Vaknin, "Intercalated rare-earth metals under graphene on SiC," J. Magn. Magn. Mater. **474**, 666–670 (2019).

[17] A. Pratt, M. Kurahashi, X. Sun, D. Gilks, and Y. Yamauchi, "Direct observation of a positive spin polarization at the (111) surface of magnetite," Phys. Rev. B **85**, 180409 (2012).

[18] Y. Harada, S. Masuda, and H. Ozaki, "Electron spectroscopy using metastable Atoms as probes for solid surfaces," Chem. Rev. **97**, 1897–1952 (1997).

[19] A. Pratt, A. Roskoss, H. Ménard, and M. Jacka, "Improved metastable de-excitation spectrometer using laser-cooling techniques," Rev. Sci. Instrum. **76**, 053102 (2005).

[20] A. Pratt, C. Woffinden, C. Bonet, and S. Tear, "Metastable de-excitation spectroscopy and scanning tunneling microscopy study of the 2 × 4 and 2 × 7 reconstructions of Ho on Si(001)," Phys. Rev. B **78**, 155430 (2008).

[21] P. Wetzel, L. Haderbache, C. Pirri, J. C. Peruchetti, D. Bolmont, and G. Gewinner, "Electronic structure of epitaxial erbium silicide films on Si(111)," Surf. Sci. **251-252**, 799–803 (1991).

[22] C. Riedl, A. A. Zakharov, and U. Starke, "Precise in situ thickness analysis of epitaxial graphene layers on SiC(0001) using low-energy electron diffraction and angle resolved ultraviolet photoelectron spectroscopy," Appl. Phys. Lett. **93**, 033106 (2008).

[23] I. Shtepliuk, V. Khranovskyy, and R. Yakimova, "Combining graphene with silicon carbide: synthesis and properties—A review," Semicond. Sci. Technol. **31**, 113004 (2016).

[24] S. Sung, S. Kim, P. Lee, J. Kim, M. Ryu, H. Park, K. Kim, B. I. Min, and J. Chung, "Observation of variable hybridized-band gaps in Eu-intercalated graphene," Nanotechnology **28**, 205201 (2017).

[25] S. Kennou, S. Ladas, M. G. Grimaldi, T. A. N. Tan, and J. Y. Veuillen, "Oxidation of thin erbium and erbium silicide overlayers in contact with silicon oxide films thermally grown on silicon," Appl. Surf. Sci. **102**, 142–146 (1996).

[26] T. Miyazaki, R. Sumii, H. Umemoto, H. Okimoto, Y. Ito, T. Sugai, H. Shinohara, T. Zaima, H. Yagi, and S. Hino, "Ultraviolet photoelectron spectra of Er2@C82 (I), Er2@C82 (III), Er2C2@C82 (I) and Er2C2@C82 (III)," Chem. Phys. **397**, 87–91 (2012).

[27] A. Siokou, F. Ravani, S. Karakalos, O. Frank, M. Kalbac, and C. Galiotis, "Surface refinement and electronic properties of graphene layers grown on copper substrate: An XPS, UPS and EELS study," Appl. Surf. Sci. **257**, 9785–9790 (2011).

[28] B. Heinz and H. Morgner, "A metastable induced electron spectroscopy study of graphite: The k-vector dependence of the ionization probability," Surf. Sci. **405**, 104–111 (1998).

[29] C. Saby, T. A. Nguyen Tan, F. Pruvost, and P. Muret, "Interfacial reaction of erbium on homoepitaxial diamond (100) films," Appl. Surf. Sci. **166**, 119–124 (2000).

[30] P. Wetzel, S. Saintenoy, C. Pirri, D. Bolmont, and G. Gewinner, "Surface states and reconstruction of epitaxial $\sqrt{3} \times \sqrt{3}$R30° Er silicide on Si(111)," Phys. Rev. B **50**, 10886–10892 (1994).